Lab on a Chip

PAPER

View Article Online
View Journal | View Issue

Cite this: *Lab Chip*, 2025, **25**, 187

OoTrap: enhancing oocyte collection and maturation with a field-deployable fluidic device†

Roksan Franko[ab] and Marcia de Almeida Monteiro Melo Ferraz *[ab]

Received 8th August 2024,
Accepted 2nd December 2024

DOI: 10.1039/d4lc00660g

rsc.li/loc

Assisted reproductive technologies (ART) are pivotal for contemporary reproductive medicine and species conservation. However, the manual handling required in these processes introduces stress that can compromise oocyte and embryo quality. This study introduces OoTrap, a novel fluidic device designed to streamline ART workflows by facilitating the capture and maturation of oocytes in a compact unit. The device also reintroduces mechanical forces similar to those in the *in vivo* environment, which are often missing in conventional systems. OoTrap operates in both static and perfusion-based modes, offering flexibility and optimal conditions for oocyte maturation. Notably, OoTrap achieved higher *in vitro* maturation (IVM) rates under perfusion, produced oocytes with fewer chromosomal abnormalities, and maintained spindle morphology integrity. The incorporation of a heating system and a 3D-printed syringe pump enabled IVM outside the incubator, making OoTrap suitable for field applications. The results highlight the potential of OoTrap to enhance ART outcomes by reducing manual handling, providing a controlled microenvironment, and offering a practical solution for field-based ART applications.

Introduction

Assisted reproductive technologies (ART) such as *in vitro* maturation (IVM), *in vitro* fertilisation (IVF), and *in vitro* production (IVP) of embryos are critical components of modern reproductive practices and conservation efforts.[1] These technologies have revolutionised reproductive medicine, offering solutions for infertility and aiding in the preservation of endangered species.[2,3] ARTs have become a crucial component of animal conservation efforts, significantly contributing to the preservation of endangered species such as the Northern White Rhinoceros and wild felids.[4,5] However, the collection of gametes from wildlife settings, including conservation programs and zoos, presents many logistical challenges. The lack of adequate supplies and the difficulties associated with transportation further complicate the effective implementation of ARTs in these environments.

Despite their widespread use and success, the manual handling required at each step of the *in vitro* gamete handling and embryo production—such as removing gametes and embryos from incubators and exchanging media—introduces significant stress, which can compromise the quality and viability of the oocytes and embryos. To address these challenges, there is a growing need for innovative devices that can streamline the workflow of ARTs while minimising handling stress. Microfluidics, which involves the manipulation of fluids at a microscale, presents a promising solution.[6,7] Microfluidic devices can offer precise control over the microenvironment, reduce contamination risks, and automate various stages of ARTs, thereby improving the overall efficiency and success rates.[8,9]

Current microfluidics models for oocyte maturation have shown promise in providing controlled environments and reducing manual handling.[10,11] Various microfluidic models for oocyte maturation have been developed (see Table S1†), utilising approaches such as microchambers, bioreactors, filter-like structures, and well membrane inserts. However, these systems have produced inconsistent results, with most showing no improvement or negative effects on oocyte maturation.[10–15] In addition to these mixed outcomes, many existing systems face significant limitations, including difficulties in loading oocytes into the device, limited scalability, and reliance on external equipment like incubators, stereomicroscopes, and perfusion pumps. These devices are designed primarily for laboratory use, which restricts their practicality in resource-limited or field-based settings. It is no surprise, then, that despite the first microfluidic device for oocyte maturation being developed over a decade ago, microfluidics has yet to become a viable option in clinical or field/farm settings.

[a] *Clinic of Ruminants, Faculty of Veterinary Medicine, Ludwig-Maximilians-Universität München, Sonnenstr. 16, Oberschleißheim, 85764, Germany. E-mail: m.ferraz@lmu.de; Tel: +49(0)89 2180 78683*
[b] *Gene Center, Ludwig-Maximilians-Universität München, Feodor-Lynen Str. 25, Munich, 81377, Germany*

† Electronic supplementary information (ESI) available. See DOI: https://doi.org/10.1039/d4lc00660g

In this context, we present two microfluidic devices tailored for oocyte capture from follicular fluid (FF) and their subsequent maturation. The first device, the OoTrap, features microwells within a dam channel and operates in both static and perfusion-based modes, thus providing flexibility and optimal conditions for oocyte maturation. This device includes an oocyte loading/media reservoir at the inlet and is connected to tubing and a syringe at the outlet, enabling the direct collection of oocytes from FF without the need for a stereomicroscope. It operates with an incubator and using a syringe pump, and mainly highlights the use of fluidic systems for automation of COC collection without the use of a microscope or a trained staff member to isolate COCs from FF. We believe this device would be of interest for any group that performs reproductive techniques on a large scale such as breeding centres and IVF clinics, that have access to specialised laboratories.

The second device we present, the heated OoTrap, maintains the same microwell structure but is smaller and more portable, making it ideal for field-based applications. The heated OoTrap integrates a self-heating system that operates with a simple power supply, eliminating the need for incubators and enabling precise temperature control even in remote settings. When coupled with a 3D-printed syringe pump, this device provides both perfusion and heat autonomously, allowing it to function efficiently without external equipment. This adaptability makes the heated OoTrap particularly valuable for wild animal conservation and other resource-limited environments, such as remote farms, conservation centers, and zoos, where oocyte collection and maturation often occur under challenging field conditions. In farm animal setups, a growing number of companies provide on-site services, collecting oocytes from live animals *via* OPU (ovum pick-up) and transporting them to the lab for IVF processing within a few hours. However, these services are typically limited to farms with specialized laboratories or locations near their labs, both of which are uncommon. The heated OoTrap addresses this limitation by extending the viable transport window to 24 hours, significantly enhancing the application of ARTs in more remote and resource-limited areas.

We evaluated the performance of both OoTrap devices in terms of fluid dynamics, cumulus–oocyte complex (COC) entrapment, IVM efficiency, and oocyte quality. Through a combination of computational simulations and experimental analyses, we demonstrated the devices capabilities in maintaining optimal culture conditions and enhancing maturation rates. Moreover, the heated OoTrap was fabricated at a low cost of approximately 26 euros per reusable unit, inclusive of a 3D-printed syringe pump and heating systems. The materials used in the devices allow for efficient cleaning and sterilisation, making them reusable. By integrating these components, we developed a portable, cost-effective, and efficient solution for oocyte collection and maturation, which is particularly advantageous for field-based settings where traditional laboratory equipment is not available.

Experimental

OoTrap design and fabrication

The fluidic devices were designed for the purpose of capturing COCs in microwells and provide constant media perfusion for the duration of culture. For this, we designed a mould using Autodesk Fusion 360 and used soft-lithography techniques with polydimethylsiloxane (PDMS) for device fabrication. The design consists of two parts: top and bottom. The top mould includes the perfusion channel and pillars for inlet and outlet on either side, and the bottom mould consists of a ramp to allow COCs to move downwards and a chamber with 135 round microwells of 750 × 500 μm (diameter × height), as shown in Fig. 1a–d. After designing, the construct was sliced using Chitubox Slicing Software (File S1†) and 3D printed in an Elegoo Saturn 3 Ultra, using a 3D printing UV sensitive clear resin (Anycubic). Following printing, the constructs were washed in 70% isopropanol (IPA) for 5 min and exposed to UV for 5 min using the Elegoo Mercury Plus.

After initial wash and curing steps, we further treated the moulds to prevent PDMS curing inhibition and for more efficiently removing any non-crosslinked remaining resin. Different protocols combining IPA washes with heating and use of ultrasonic treatment were tested (see Table S2† for details), and the best approach is described here. For this, 3D printed moulds were submerged in absolute IPA and were placed in an ultrasonic bath for 15 min in sweep mode at 45 kHz (Transsonic multi-frequency ultrasonic cleaning unit, Elma, Germany). After drying off excess IPA, moulds were placed in the oven at 100 °C for 1 h, followed by another ultrasonic bath wash for 15 min submerged in absolute IPA, moulds were then air dried and used for PDMS casting.

After complete curing and washes, these moulds were used for soft-lithography using PDMS. For this, PDMS (Sylgard 184, Dow Corning) was mixed with the curing agent at a 10 : 1 ratio. After desiccation, PDMS was poured into the moulds and desiccated further until no air bubbles were visible. Moulds filled with PDMS were then cured at 100 °C for 30 min. The two parts of PDMS were removed from the moulds, plasma treated for 15 s at 100% power (PiezoBrush PZ3, Relyon Plasma GmbH, Germany), assembled and incubated for 30 min at 100 °C with weight on top.

Once the device was ready for final assembly, a 5 mL reservoir (Microfluidic ChipShop, Germany) was placed in the inlet hole, and the outlet hole was connected to the tubing (1.27 i.d. × 2.29 o.d. mm), which was attached to a syringe (Thermo Fisher Scientific) with a 19G blunt needle. All steps performed to fabricate the OoTrap are shown in Fig. 1e and the final device is shown in Fig. 1f.

Prior to use, devices were cleaned by adding 5 mL of sterile ultra-pure water in the inlet reservoir and withdrawing it from the outlet. This wash was repeated three times with

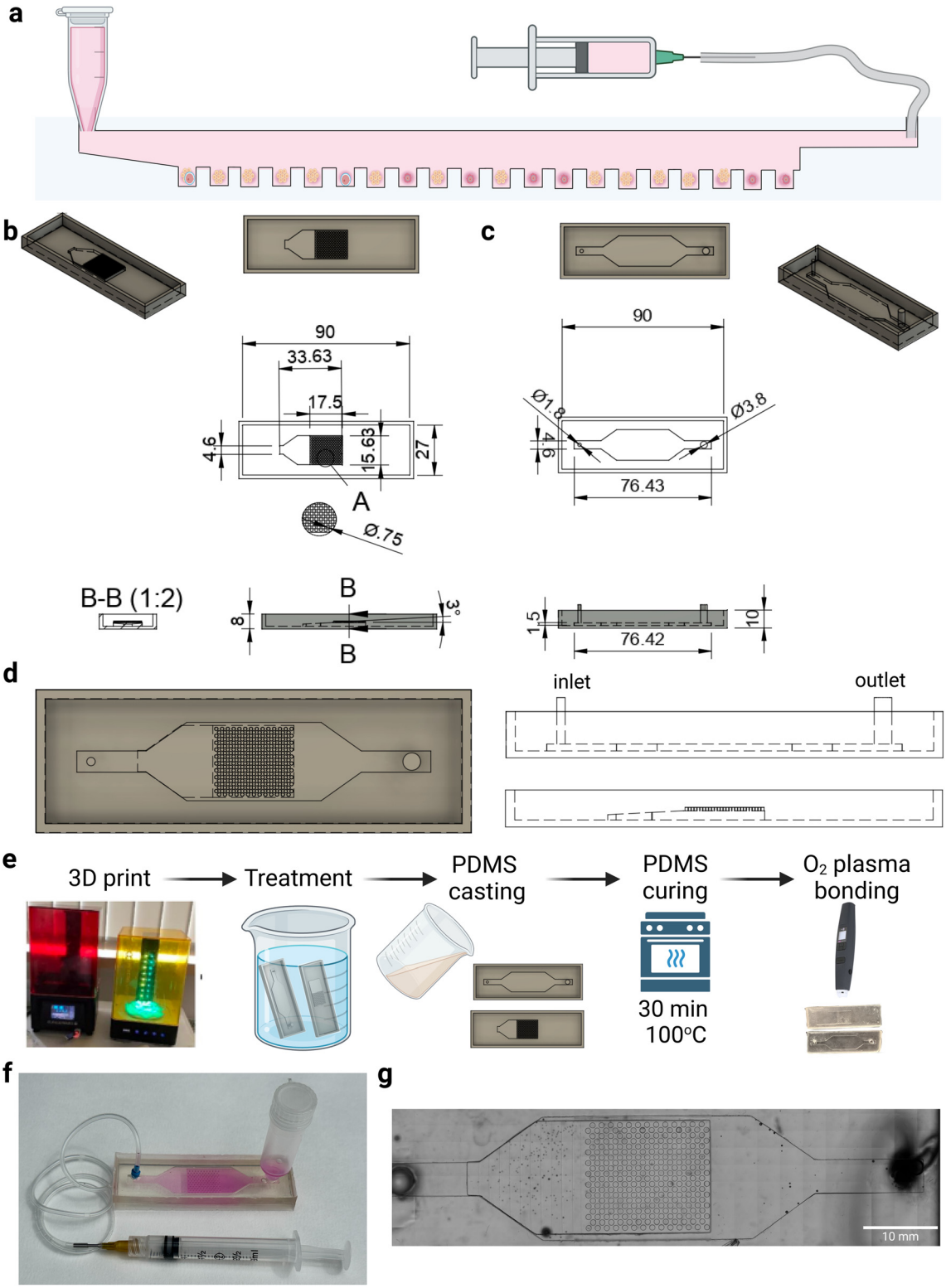

Fig. 1 Design and fabrication process of the OoTrap device. In (a), schematic drawing of the fluidic device setup, designed for capturing COCs in microwells and providing constant media perfusion. The design consists of a bottom mould (b) featuring a dam and a chamber with 135 microwells, each measuring 750 × 500 μm (diameter × height); and a top mould (c) with a perfusion channel and inlet/outlet pillars. Lateral views of both moulds can be seen in (d), the assembly includes the inlet and outlet for media perfusion. The fabrication process involves several steps as shown in (e): 3D printing the moulds using a UV-sensitive clear resin, treating them with IPA and UV light, casting PDMS into the moulds, curing the PDMS, and performing oxygen plasma bonding to assemble the parts. The final assembled OoTrap device is equipped with a 5 mL reservoir and connected to tubing for perfusion (f). In (g), a light microscopy image of the full device and microwells is displayed, illustrating the detailed structure designed for efficient COC trapping. Dimensions presented are in mm.

ultra-pure water, three times with 70% ethanol, and three times with water again. During the first water wash and ethanol wash, devices were also UV treated for 15 min each, using the laminar flow UV (StellaAir, Zefa, Germany). All steps were performed inside the laminar flow. All parts of the device were then autoclaved prior to their use for experiments. Before use for IVM, devices were filled with wash media (medium 199 supplemented with 10% FBS, 105 mM HEPES, 50 μg ml^{-1} gentamicin, and 0.2 mM sodium pyruvate) and incubated overnight at 38.5 °C, 5% CO_2 and atmospheric air under 20 μL h^{-1} flow rate.

Computational fluid dynamics (CFD) modelling and simulations

Computational modelling of flow dynamics, shear stress, and diffusion of particles within the OoTrap device was conducted using COMSOL Multiphysics 6.1 (COMSOL Inc., MA, USA). The .stl file containing the 3D design of the OoTrap was imported into COMSOL, where the inlet and outlet regions were specified. 3D CFD simulations were performed using 'Laminar Flow' physics from the CFD Module. No-slip boundary conditions were chosen for the walls and water was chosen as a fluid for the simulation (μ = 1 mPa s ρ^{-1} = 1000 kg m^{-3}). Fluid was introduced perpendicular to the inlet channel with a flow rate of 20 μL h^{-1}, while no back pressure was used for the outlet. Oocytes were simply modelled as rigid and non-deformable spheres in the fluidic domain. The shear rate over the sphere surfaces was calculated by using the shear rate components surrounding the *x*-, *y*- and *z*- directions. After simulations, the shear rates over the range of 500 μm surrounding the sphere surface were obtained and maximum, minimum and average shear rates were determined.

A 3D time-dependent simulation of bovine serum albumin (BSA) and hydrogen peroxide (H_2O_2) diffusion in the OoTrap was performed using a finite element method (FEM)-based CFD. The diffusion coefficient of BSA and H_2O_2 in the medium was assumed to be the same as that in water (1 × 10^{-9} m^2 s^{-1} and 1.43 × 10^{-9} m^2 s^{-1}, for BSA[16] and H_2O_2,[17] respectively). The initial concentration of BSA in the medium in the channel was set to 1 mol m^{-3}, in the microwells was assumed to be 0, and a 1 mol m^{-3} BSA solution was set to be perfused at 0 and 20 μL h^{-1} flow rates. For the analysis of H_2O_2 clearance, the initial concentration of H_2O_2 was set to be 1 mol m^{-3} in the microwells and 0 in the channels; a 0 mol m^{-3} solution was set to be perfused at 0 and 20 μL h^{-1} flow rates. The diffusion was estimated in a time-dependent CFD.

To validate media exchange, we conducted a fluorescein diffusion assay within the OoTrap. The device was initially filled with a fluorescein solution at a concentration of 2 μg mL^{-1}, and perfused at a flow rate of 20 μL h^{-1} using a fluorescein-free solution. Time-lapse images were acquired every 30 min over the course of 24 h, using an EVOS M7000 microscope with a ×4, NA 1.25 objective. The fluorescein was measured at a 482/25 nm excitation LED light cube. Imaging was performed in three distinct regions: the inlet and microchannels with imaging focused on the centre of the channel (IN), the outlet region with imaging focused on the centre of the outlet channel (OUT), and the microwell region with imaging focused on the centre of the microwell (MW; n = 3 devices). Fluorescence intensity in each region was measured using ImageJ software. For the IN and OUT regions, the full areas were analysed, while the microwells were individually delimited by circles previously to measurement. The fluorescence at time point 0 was set as 100%, and the decrease in fluorescence over time was normalised relative to this baseline value.

A 3D time-dependent simulation of fluorescein dye diffusion in the OoTrap was conducted using finite element method (FEM)-based computational fluid dynamics (CFD). The diffusion coefficient of fluorescein in the medium was assumed to be the same as in water (4.25 × 10^{-6} cm^2 s^{-1}).[18] The initial concentration of fluorescein in both the channel and microwells was set to 1 mol m^{-3} while a 0 mol m^{-3} solution was perfused at a flow rate of 20 μL h^{-1}. The diffusion process was simulated over a 24 h period using time-dependent CFD. To compare with the experimental data, the simulation results were analysed separately for the three regions: inlet (IN), outlet (OUT), and microwell (MW).

Viscosity measurements of IVM media and shear stress calculation

The viscosity of IVM media was measured using the microVROC (Rheosense, Inc.; San Ramon, California, USA). Samples were equilibrated to room temperature (RT) for at least 60 min before measurement. Viscosity measurements were conducted using 400 μL pipettes and the A05 chip, with advanced mode applied to access different shear rates while keeping priming and measurement volume automatic. Initially, viscosity was measured at shear rates of 8000, 4000, and 2000 s^{-1}. Due to the Newtonian nature of the fluid, a shear rate of 8000 s^{-1} was selected. Measurements were considered valid if classified as stable ($R^2 > 0.98$) and if the standard error of repeated measurements was <10%.

To calculate shear stress in the OoTrap, we used the shear rate obtained from COMSOL simulations along with the measured viscosity of the IVM media. The formula for shear stress (τ) is:

$$\tau = \eta \cdot \gamma$$

where:

τ is the shear stress (Pa),

η is the dynamic viscosity (Pa s),

γ is the shear rate (1/s).

Initially, shear stress was calculated in Pa using the measured viscosity and simulated shear rate. To make the results comparable with existing literature, we converted the

shear stress values from Pa to dyne cm^{-2} by using the conversion factor 1 Pa = 10 dyne cm^{-2}.

COCs collection, OoTrap loading and IVM

Bovine ovaries were collected from the local abattoir and transported to the laboratory within 3 h at RT. The ovaries were washed in physiological saline (0.9% w/v NaCl) and held in physiological saline containing 100 U ml^{-1} penicillin and 100 μg ml^{-1} streptomycin at 30 °C. FF and COCs were aspirated from follicles with a diameter of 2 to 8 mm and collected into 50 mL conical tubes using a 19-gauge needle and a vacuum pump.

For IVM experiments with OoTrap, 5 ovaries per device (or well for control) were aspirated. For selected COC experiments, 50 COCs with three layers of intact cumulus cells were selected and added into the reservoir of the OoTrap. In non-selected groups, FF was left to settle after aspiration, and 2 mL of the FF sediment was added into the inlet reservoir of the OoTrap. The FF was allowed to enter the device by aspirating the fluid using the syringe connected to the outlet manually. To allow efficient settling of COCs in microwells, the 3 mL syringe was withdrawn by hand 500 μl at a time within 2–3 s, followed by a wait of 30 s after each aspiration to allow COCs to settle before another fluid withdrawal. Care was taken to prevent bubble formations in the device by adding wash media in the reservoir as needed. To remove cell debris more efficiently, the devices were slightly tilted sideways to wash away bigger particles. Table S3,† depicts the step by step for loading and unloading of COCs. Once COCs settled and cell debris were removed, wash media was exchanged with IVM media (M199 supplemented with 0.1 IU mL^{-1} follicle stimulating hormone, 10% FBS, 2.5 μg mL^{-1} gentamicin, and 0.2 mM sodium pyruvate). In control groups, either all or good quality COCs were collected, washed twice in wash media and once in IVM media, and were transferred to 4-well plates with 500 μL of IVM media, in line with common IVM procedures. IVM was performed for 22–24 h in an incubator at 38.5 °C, 5% CO_2 and atmospheric air, under dynamic (20 μL h^{-1} or 0.0005 mm s^{-1}), static, or control (4-well plate) conditions.

To determine the COC entrapment efficiency of OoTrap, we collected all FF and media after loading to assess the presence of COCs, indicating any loss during the trapping process. To do that, the contents of the tubing and the syringe were emptied into a petri dish and we counted the number of COCs found under a stereomicroscope to determine whether and how many COCs were lost during these processes. For evaluating mature COCs loss during removal from OoTrap, we first counted the number of COCs recovered post-IVM. Subsequently, we counted the COCs that remained inside the device by checking the microwells under a microscope. This two-step counting process allowed us to accurately gauge COCs loss during the removal phase, providing a comprehensive evaluation of the device's performance.

Immunofluorescence

COCs were collected after 22–24 h in IVM, denuded by pipetting with hyaluronidase solution (30 mM in wash media, MP Biomedicals, USA), fixed with 4% paraformaldehyde (PFA) for 30 min and were stained with 5 μg mL^{-1} Hoechst 33342 (Thermo Fisher Scientific) for 30 min. After washing with PBS, oocytes were mounted on a microscope slide and maturation status was evaluated on an EVOS M7000 (Thermo Fisher Scientific), using a ×40 objective with 0.45 NA, LED light cube with excitation (Ex): 357/44 and emission (Em): 447/60.

For determining the chromosomal integrity and spindle morphology, COCs were collected and fixed as previously mentioned. COCs were incubated in a blocking and permeabilization solution (0.1% Triton X-100, 2% BSA in PBS) for 1 h at RT, stained with 5 μg mL^{-1} Hoechst 33342 and FITC-labelled anti-α-tubulin (1 : 100, Merck) in PBS solution containing 0.1% PVP overnight at 4 °C. The next day, oocytes were washed three times in PBS-PVP (0.1%) for 5 min each and mounted on slides with an antifade mounting solution (ProLong Diamond Antifade Mountant, Invitrogen). Oocytes were then imaged using a laser scanning confocal microscope Leica SP8 (Leica Microsystems GmbH, Wetzlar, Germany) attached to an inverted semi-automated DMI4000 microscope (Leica) with a ×40, NA 1.25 objective. The spindle marker (α-tubulin) was excited at 482/25 nm and emitted at 524/24 nm, while the nuclei were excited at 357/44 nm and emitted at 447/60 nm. *Z*-Stacks were acquired with 1 μm steps to reconstruct the spindle and assess chromosome alignment and spindle morphology. ImageJ software was used to create 3D projections of the *Z*-stacks for detailed analysis.

Field-compatible heated OoTrap design and fabrication

This fluidic device was designed for better compatibility for field-collection settings. Therefore, a smaller and circular design was made [38 × 8 mm (diameter × height)] with 78 microwells (750 × 500 μm, diameter × height). Similarly to the original OoTrap, 2 separate parts of moulds were 3D printed and treated, and were used for PDMS casting. The same fabrication protocols were used to produce these heated devices. To achieve heating of the culture media inside the PDMS device to 38.5 °C, we employed Joule heating using a nichrome wire. The nichrome wire, with a diameter of 0.25 mm, was arranged in a flower shape within the PDMS device, as depicted in Fig. 4a and b. This configuration was specifically chosen to ensure even heat distribution across the device. The total length of the wire was 28–30 cm in the top and 22–25 cm in the bottom part. The PDMS device was fabricated as described above, ensuring that the embedded nichrome wire was securely encapsulated within the PDMS matrix.

The nichrome wire was then connected to a DC–DC step down converter module, an adjustable buck converter

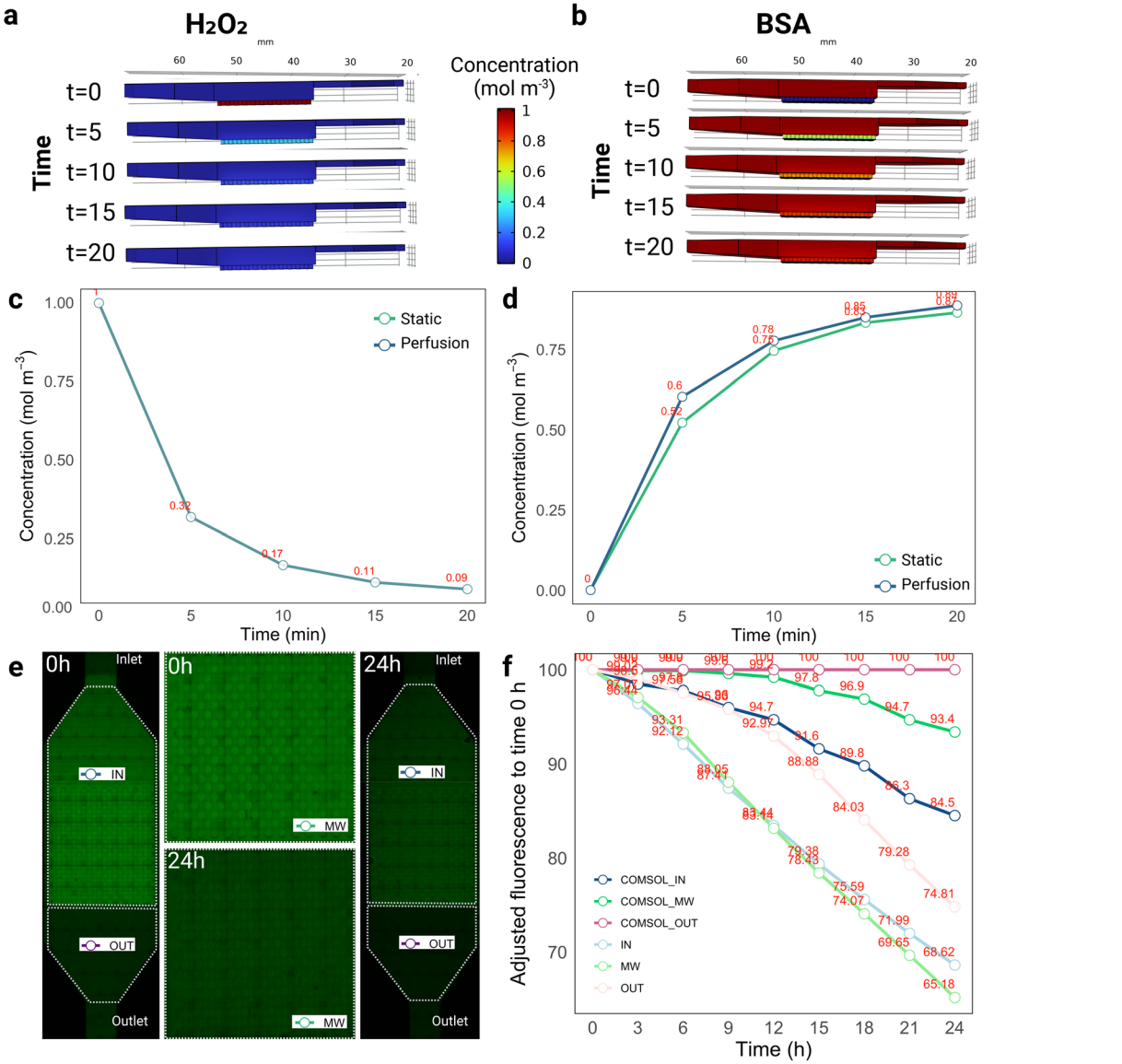

Fig. 2 Simulations of diffusion in the OoTrap device. In (a), and (b), COMSOL simulation of changes in concentration of hydrogen peroxide (H_2O_2) and BSA, respectively, within the microwells under perfusion conditions (20 μL h^{-1}) is shown. In (c), the drop in concentration of H_2O_2 in the microwells is plotted over time under both static and perfusion conditions (20 μL h^{-1}), showing efficient simulation of diffusion out of wells. Similarly, in (d), the simulated concentration of BSA in the microwells over time is shown under static and perfusion conditions (20 μL h^{-1}), indicating that media components efficiently enter the microwells. In (e), we show the experimental testing of fluorescein dye diffusion from the OoTrap device, highlighting the three regions analysed: the inlet and microchannels with imaging focused on the centre of the channel (IN), the outlet region with imaging focused on the centre of the outlet channel (OUT), and the microwell region with imaging focused on the centre of the microwell (MW). Time-lapse imaging of these regions and their respective focal planes was conducted over 24 h. Representative images from 0 hours and 24 hours are displayed in (e), with fluorescence quantification (n = 3 devices) over time as well as COMSOL simulations of each location shown in (f). Red values in (c), (d) and (f) indicate mean values.

module with a LED display. This module allowed us to precisely control the voltage applied to the nichrome wire. To determine the required voltage to achieve this temperature within the PDMS device, we tested different combinations of voltage and current. To do that, the temperature of the culture media inside the channel was monitored using a temperature sensor inserted inside the channel and a Proster Digital Thermometer with dual-channel K-type thermocouples. To validate temperature stability over time, we measured the temperature over a course of 90 min, recording the temperature every 5 min.

3D-printed syringe pump for field application

This model was based on a syringe pump model from Thingiverse (**https://www.thingiverse.com/thing:2797132**, accessed on June 2nd, 2024), which was adapted to accommodate a 1 mL syringe. The modifications include

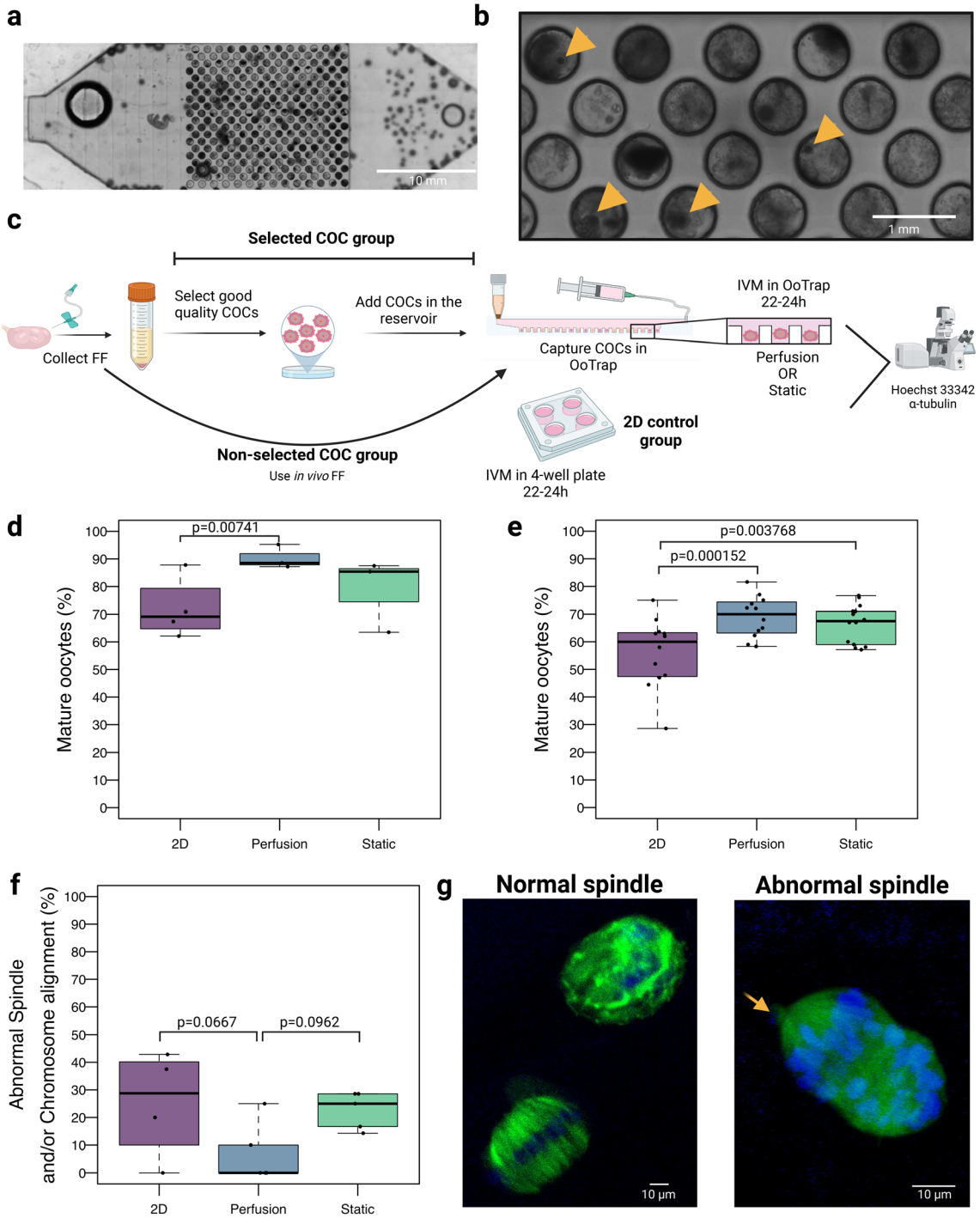

Fig. 3 IVM in OoTrap. In (a), COCs are shown trapped in the microwells of the OoTrap, and a zoom in of microwells with arrowheads indicating the COCs is shown in (b). In (c), the experimental setup is detailed for both selected COC experiments and FF non-selected experiments, showing the steps from collecting FF to capturing COCs in the OoTrap and conducting IVM. Boxplot depicting maturation rates for selected COCs (d) and non-selected (e) are presented, comparing control (2D), static, and perfusion cultures. In (f), spindle integrity and chromosomal abnormalities in metaphase II (MII) oocytes are compared across the groups. In (g), examples of normal and abnormal spindle morphology and chromosome alignment are shown; the arrow indicates a misaligned chromosome.

designing a customised base to securely hold the 1 mL syringe, ensuring stability and accuracy during fluid dispensation. The primary objective of this adaptation was to achieve a precise flow rate of 20 µL h^{-1}.

The syringe pump system integrated a stepper motor connected through a series of geared wheels, culminating in an actuator arm fitted with precision spikes that translate rotational motion into linear displacement. This setup was

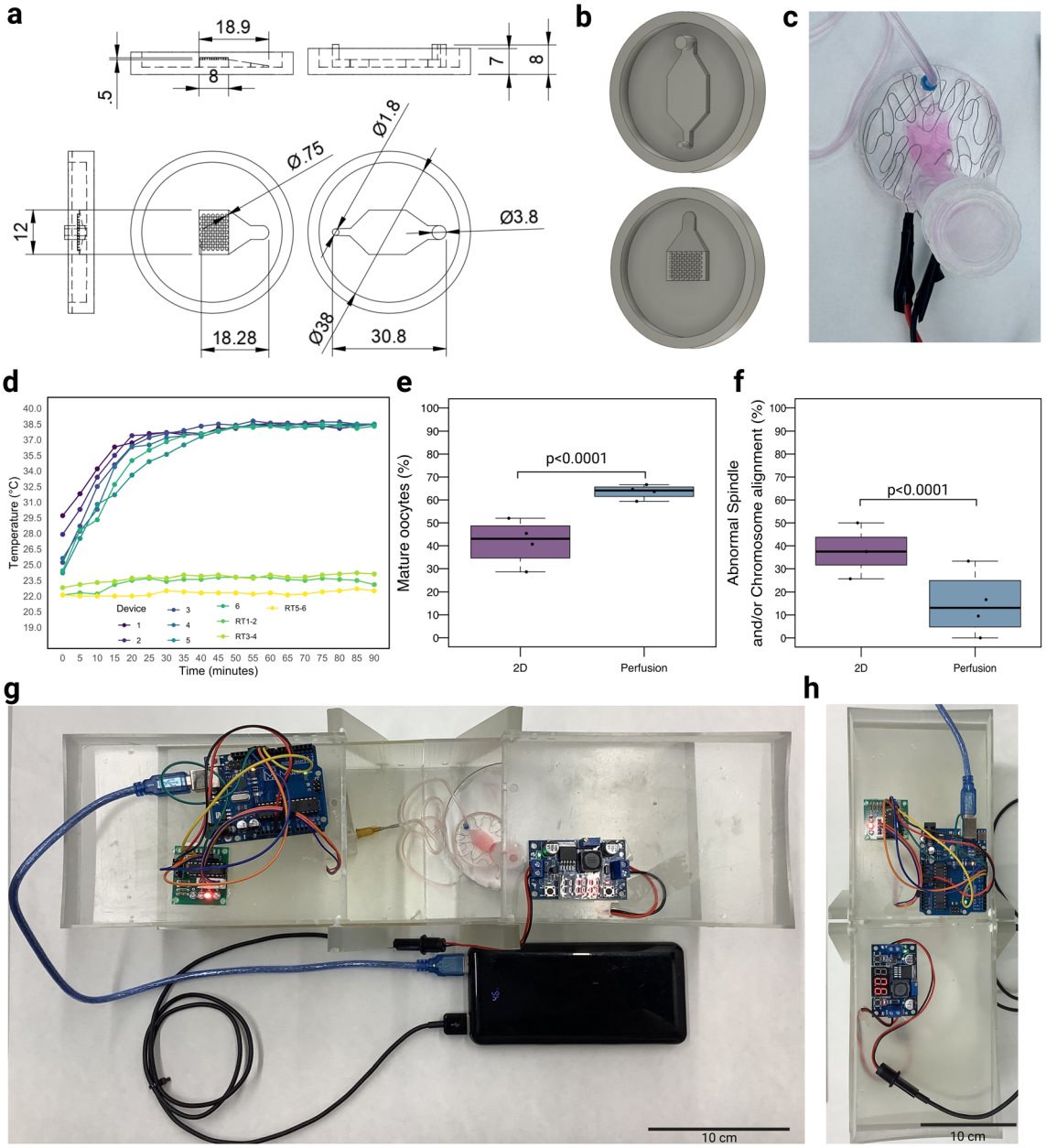

Fig. 4 Field-friendly OoTrap. In (a), detailed dimensions and Fusion 360 models of the smaller OoTrap version are shown, along with the 3D model of the mould (b). In (c) the flower-shaped pattern of the nichrome wire is displayed, covering most of the device's surface, both on the top and bottom, to provide localised and efficient heating. The temperature profile of the OoTrap was measured over a course of 90 min in 6 devices, demonstrating consistent temperature maintenance within the range of 38.1–38.5 °C, achieving stability in approximately 35 minutes; room temperature (RT) was also measured for comparison (d). In (e), boxplot depicting maturation rates of non-selected COCs under 2D and perfusion conditions. In (f), spindle integrity and chromosomal abnormalities in MII oocytes are compared between the groups. The portability of the heated OoTrap was enhanced by designing a custom transport box to hold all electrical and non electrical components (g), which can be easily closed to form a humidified chamber, protect from light and facilitate its transport (h). Dimensions presented in (a) are in mm.

specifically designed for precise fluid dispensation. The configuration included a motor wheel with a pitch diameter of 10 mm and 16 spikes, a transmitter wheel with 32 spikes and a pitch diameter of 24 mm, and a second wheel with 12 spikes and a pitch diameter of 8 mm. The actuator arm, 90 mm in length, features 36 spikes spaced at 2 mm intervals, directly interfacing with the syringe plunger. Detailed calculations were performed to determine the necessary delay between motor steps, ensuring consistent and accurate fluid flow (File S1†).

COCs loading and IVM in the field-compatible heated OoTrap

The new OoTrap device was sterilised and prepared following the same protocol as the original OoTrap. For IVM

experiments, oocytes from 5 ovaries per device were aspirated as described previously and loaded into the device with slight modifications (Table S4†). The maturation media was supplemented with 75.5 mM HEPES to maintain pH control outside the incubator. The devices were placed inside pipette tip boxes on top of a wet clean room tissue (one tissue plus 20 mL of sterile ultra-pure water) and subjected to IVM at a flow rate of 20 μL h^{-1} (0.001 mm s^{-1}) for 22–24 h on the bench. As a control, IVM was also performed in a 2D well setup inside an incubator at 38.5 °C, 5% CO_2, and atmospheric air for 22–24 h. COCs were collected after 22–24 h in IVM, denuded, fixed with 4% PFA for 30 min and stained as described above.

Statistical analysis

All data analyses and visualisation were carried out in R (ver. 4.3.1), and the scripts and packages used for carrying out our analyses are described in File S2.† Visualisations included detailed boxplots with jittered data points overlay to show the distribution and individual variability in oocyte maturation and morphology across different conditions. Line plots were created to visualise temperature variations. To analyse the effect of different treatments on maturation and spindle morphology, a generalised linear mixed model with a beta distribution was employed. The model was fitted using the glmmTMB function from the glmmTMB package in R. The response variable was the proportion of maturation/abnormal spindle, expressed as a percentage, and the predictor variable was the treatment group. A random effect for replicate was included to account for variability between replicates. Model fit and assumptions were assessed using the DHARMa package, which provided diagnostic checks for residuals to ensure the models were appropriately specified.[19] To further investigate the pairwise differences between treatment groups, a Tukey *post hoc* test was conducted. The significance level was set at $\alpha = 0.05$.

Results and discussion

OoTrap fabrication

The OoTrap device was fabricated using 3D printed moulds, which allow for rapid adaptation and quick production of PDMS devices. For this, a design to allow capture of COCs from FF was made, consisting of a dam and a microwell base (Fig. 1a). To produce this device, we designed and 3D printed two moulds: top and bottom (Fig. 1a–d). Our workflow for the fabrication of devices is shown in Fig. 1e. Briefly, the parts were printed and were subjected to treatment as described in our methods. Following treatment, PDMS was prepared, transferred to moulds and cured at 100 °C. After, cured PDMS pieces were removed from moulds, were bonded to each other using plasma treatment, and reservoir and outlets were included (Fig. 1e and f). This approach significantly reduced the time and cost associated with traditional SU-8 mould fabrication. With this fabrication procedure, we can 3D print the moulds in just 20 min at a cost of ~0.50 euro each, which is particularly advantageous during the early stages of development when frequent design modifications are needed. This process allowed us to modify the design, print, treat the mould, and produce PDMS devices all within half a day—a significant advantage over traditional SU-8 wafer fabrication. Additionally, since the moulds are reusable and PDMS curing takes only 30 min, we can produce multiple devices from the same mould in a single day. However, one challenge with 3D printed moulds, especially those created using stereolithography, is that they can release uncured substances that interfere with the curing of PDMS.[20] To address this, we tested various treatments to ensure proper PDMS curing (Table S2†). Different resins and treatments were tested to find the optimal conditions for PDMS curing, including: Elegoo ABS-like red, Elegoo standard black, Elegoo plant-based grey, Elegoo water washable, Anycubic black, Anycubic clear, 3DMaterials SuperFlex, and Nova3D high transparency. Treatments included combinations of IPA washing, UV exposure, and heat treatment. For the best results, Anycubic clear resin with a 15 min ultrasound bath incubation in pure IPA followed by 1 h at 100 °C and another 15 min ultrasound bath incubation in pure IPA was found to be most effective. Despite these efforts, the first PDMS casting often needed to be discarded due to incomplete curing leading to PDMS stickiness.

The toxicity of most commercial 3D printing resins is another well-documented problem. Our previous assessments of five common polymers used in 3D printing and prototyping showed significant toxic effects on early bovine embryo development and oestrogen receptor activation.[21] Additionally, we have previously shown that moulds produced by stereolithography can indeed leach various components into PDMS. Leachates detected in aqueous solutions incubated in PDMS devices prepared with common PDMS pre-polymer agent ratios (10 : 1, 15 : 1, and 20 : 1) originated from resins and catalyst substances.[22] Subsequent experiments demonstrated that, after proper washing and conditioning, PDMS devices from 3D printed moulds could support the physiological culture of HeLa cells and ovarian tissues, achieving better outcomes than static conventional cultures.[22] Here, to prevent these toxic effects, we performed multiple washes with water and ethanol 70%, and left the devices under perfusion in IVM medium overnight before use.

CFD simulations confirm efficient diffusion and low shear stress in OoTrap

Microfluidics play a crucial role in biomedical applications by enabling precise control over the microenvironment, which is essential for processes such as nutrient diffusion and waste removal. In microfluidic devices used for cell culture, maintaining an optimal environment ensures that cells receive the necessary nutrients while metabolic wastes are efficiently removed. This balance is vital for cell viability

and function, particularly in sensitive applications like oocyte maturation and embryo culture.

Our simulation studies using COMSOL Multiphysics provided further insights into the performance of the OoTrap device. For this study, an initial concentration of H_2O_2 and BSA were assigned within the microwells as 100% and 0%, respectively, and changes in concentration were observed over time. After 20 min under both static and perfusion conditions, more than 99% of H_2O_2 was removed from the microwells (Fig. 2a and c). The simulations demonstrated that H_2O_2, a common by-product in cellular environments, can be efficiently cleared from the microwell, independent of the flow rate (Fig. 1c). Additionally, the diffusion of molecules into the microwells was efficient, with BSA as a model protein showing more than 87% diffusion to microwells under static and perfusion conditions (Fig. 2b and d). In the case of this bigger molecule, the perfusion had a slightly higher diffusion than static conditions. This high efficiency of diffusion and clearance is significant for maintaining optimal culture conditions, as it ensures that oocytes are not exposed to harmful waste products, that can be potentialized due to the presence of a high number of follicular cell debris.

To validate the COMSOL simulations, we investigated the diffusion of fluorescein during perfusion of the OoTrap in three different regions. After 24 h, 31.4, 25.3 and 34.8% clearance was observed in the IN, OUT and MW regions, respectively (Fig. 2e and f). It is noteworthy to mention that perfusion and media exchange in our setup are low; with the current flow rate of 20 μL h^{-1}, approximately 480 μL of media is exchanged over 24 h, which is not enough to promote a complete media exchange within the device. This is reflected in the 25–35% reduction in fluorescein, indicating that clearance is incomplete. A comparison between the time-lapse experimental data and the COMSOL simulations for fluorescein diffusion revealed that the modelled diffusion was slower than what was observed in the OoTrap experiment (Fig. 2f). This discrepancy highlights the need for caution when relying solely on computer modelling, as simulations may not fully capture the complexity of experimental conditions.

Another crucial factor influencing the development of oocytes and embryos is shear stress. Previous research has indicated that high shear stresses (>1.2 dyne cm^{-2}) can adversely affect mouse embryo development by triggering stress-activated protein kinase-mediated apoptosis.[23] Early-stage embryos (8–16 cells) are particularly susceptible compared to blastocysts. In our previous work using an oviduct-on-a-chip, we have demonstrated that embryos could experience shear stress as high as 2.06 dyne cm^{-2}, exceeding the threshold shown to impact embryo development negatively, which could have been responsible for the lower embryo rates observed.[24] The initial shear stress experienced by the oocytes in the OoTrap occurs during the loading of the COCs, both under static and dynamic conditions. However, due to the brief exposure to this shear stress (5–10 cycles of 2 s each, with 30 s intervals), we believe it is unlikely to influence the oocytes. Previous study has shown that continuous shear stress over 6 to 12 h can impact embryo development, with shorter durations, such as 6 h, having milder negative effects. To model shear stress within the OoTrap during the 24 h IVM, we incorporated a solid sphere in the microchannel design in COMSOL, sized to mimic an oocyte (Fig. S2†). We then analysed the shear rate around this structure under static and perfusion conditions, and calculated the maximum, minimum, and average shear stress on the surrounding surface, by using the IVM media viscosity, measured at 0.94 ± 0.16 mPa s. Under perfusion, the simulated average shear stress in the OoTrap was 0.0449 dyne cm^{-2}, with a maximum of 0.148 and a minimum of 0.00191 dyne cm^{-2}. While under static condition, the shear stress was constantly low at 1.4×10^{-7} dyne cm^{-2} (Fig. S2†). None of the analysed shear stress values exceeded the detrimental threshold at the flow rate used, confirming the suitability of the OoTrap for oocyte maturation.

OoTrap effectively collects COCs without the need of a stereomicroscope

The OoTrap device was specifically designed to facilitate the collection of COCs without the need for stereomicroscope or specialised personnel. This user-friendly design allowed for easy loading of oocytes directly into the device, making it accessible for use in field settings or by individuals without extensive training. The process of loading COCs into the OoTrap involved adding FF containing the COCs directly into the device in approximately 5 min. Although adding all the FF ensures low COCs loss, it also introduces a significant amount of cell debris into the device. While cell debris does not appear to impact IVM efficiency, it can obscure visibility and make it more challenging to retrieve COCs after maturation. An image of the microwell area with captured COCs is shown in Fig. 3a.

The OoTrap demonstrated high trapping efficiency, with a recovery rate of 87.7 ± 4.4% (n = 17 devices). This indicates that most COCs added to the device are successfully captured and retained for maturation. Of the 12.3% COCs lost, about 70% were either degenerating, denuded, or had expanded cumulus cells. A similar efficiency was observed during mature COCs removal from the device, with a recovery rate of 91.7 ± 11.5% (n = 7 devices). The 8.3% loss after maturation is attributed to the strong attachment of cumulus cells to the microwells, which complicates removal using the developed protocol. To mitigate this attachment of COCs to the PDMS microwells, various PDMS coating methods could be employed. Such as coating the PDMS surface with polyethylene glycol (PEG), which is known to reduce protein adsorption and cell attachment due to its hydrophilic nature,[25] polydopamine coating, which can provide a more biocompatible surface, reducing non-specific binding,[25] as well as Pluronic F-127 that can create a non-adhesive layer,

which could minimise COCs adhesion.[26,27] Exploring these coating techniques could enhance the removal efficiency of COCs from the OoTrap device.

Perfusion leads to increased rates of oocyte maturation and normal spindle

Ovarian follicles and the COCs experience various mechanical forces, including hydraulic and hydrostatic pressure, shear stress, and compressive stress, which can influence oocyte growth and development.[28] Follicle rupture and ovulation are driven by physical forces as hydraulic pressure within the FF and hydrostatic pressure by the follicle walls increase. Coupled with enzymatic degradation of the extracellular matrix, rupture of follicle during ovulation depends on these mechanical forces.[28,29] Shear stress from fluid flow within the follicle impacts cellular signalling pathways, and compressive stress from surrounding follicular cells affects cellular mechanics and structural integrity. Such mechanical forces are sensed by cells surrounding the oocyte and influence mechanotransduction pathways that alter many crucial cellular processes including apoptotic, differentiation and survival mechanisms.[30] In fact, Rashidi *et al.* showed improved maturation rate in mice *in vitro* when maturation was performed in a pressure chamber, introducing hydrostatic pressure upon the oocytes.[29,31] Due to the limited understanding of the forces involved in bovine *in vivo* oocyte maturation, accurately simulating these forces *in vitro* remains challenging. Nevertheless, with the OoTrap, we can reintroduce some of these mechanical forces—particularly explored here was the shear stress—which are often absent in conventional systems, representing a significant step forward in mimicking the natural follicular conditions during IVM.

To investigate the impact of OoTrap on oocyte maturation and spindle morphology, we conducted experiments under different conditions: 2D, static, and perfusion (Fig. 3c). Initially, we selected good quality COCs and evaluated their maturation rates under the different treatments. The perfusion group (n = 133, 3 replicates) showed a significantly higher mean maturation rate of 90.32 ± 4.32% compared to the 2D (n = 188, 3 replicates), while it was not statistically different form the static group (n = 155, 3 replicates), which had mean maturation rates of 72.04 ± 11.11% and 78.80 ± 13.29%, respectively (Fig. 3d). These results suggest that perfusion provides a more favourable environment for oocyte maturation. Most of the microfluidics models used in oocyte biology have been focusing on oocyte cryopreservation,[32–37] with only few studies checking for oocyte maturation and oocyte quality.[11–14,38,39] As shown in Table S1,† IVM in microfluidic models has been explored across various species including mice, cows, sheep, and pigs. Notably, the outcomes of these studies have been variable. For instance, mouse[38,39] oocytes exhibited a 27% increase in maturation rates, while pig[40] oocytes showed a 10% increase. Conversely, some studies reported decreased maturation rates in porcine[13] and sheep[11] oocytes when using microfluidic systems. Interestingly, by encapsulating sheep oocytes into microbeads, the same authors were able to mitigate the negative effect of perfusion on IVM, although this approach induced increased oxidative stress.[12] In cow oocytes, no significant effects on maturation were observed when using microfluidic systems.[14] However, while maturation rates remained unchanged, bovine oocytes matured in these devices exhibited lower blastocyst formation rates. In our study with selected COCs, we observed an 18% increase in oocyte maturation, comparable to the results seen in mouse oocytes. Unlike studies reporting reduced or negligible effects on oocyte maturation, our study used lower linear flow (0.0005 mm s^{-1}). In contrast, other studies employed higher linear flow, up to 0.01 mm s^{-1}, which could have introduced higher shear stress, negatively impacting oocyte development. This suggests that adapting perfusion rates in microfluidic systems may be crucial to minimising shear stress and promoting better oocyte maturation outcomes.

Subsequently, we assessed maturation rates without selecting oocytes, performing 13 replicates for each group. The perfusion group (n = 485 COCs) again demonstrated the highest mean maturation rate of 69.02 ± 7.39% compared to the 2D (n = 328 COCs) and was no different form the static (n = 347 COCs) group, which had mean rates of 56.04 ± 12.62% and 66.54 ± 6.94%, respectively (Fig. 3e). This consistent trend underscores the advantages of perfusion in enhancing oocyte maturation rates, likely due to improved nutrient and waste exchange, as well as the introduced mechanical forces facilitated by dynamic fluid flow.

We also examined spindle morphology and chromosome alignment abnormalities in metaphase II (MII) oocytes across the different treatment groups. The perfusion (n = 64 oocytes) group exhibited a trend to have lower abnormalities at 7.00 ± 10.95% compared to the 2D (n = 38 oocytes) and static groups (n = 50 oocytes), which had abnormalities of 25.09 ± 19.36 and 22.63 ± 6.73%, respectively (Fig. 3f and g). Our results demonstrate that the dynamic environment provided by our fluidic device, better mimics the *in vivo* environment and shows a reduced occurrence of chromosomal abnormalities and improved spindle morphology, which are critical for successful oocyte maturation and subsequent embryonic development.[41,42] This can be explained by the inherent mechanical nature of cell division, where cellular mechanics critically determine the cell shape changes necessary for progression through the cell cycle.[43] The interplay between biochemical signals, cell shape, and cellular mechanics orchestrates cytokinesis and other morphogenesis events.[44] In our fluidic model, the mechanical forces and fluid flow likely provide mechanical cues similar to those present *in vivo*, which are essential for the proper orientation and function of the mitotic spindle. Additionally, mechanical forces transmitted through cellular structures such as integrins, cytoskeleton, and nuclear scaffolds play a crucial role in ensuring the stability and functionality of the spindle

apparatus.[45] The reduced tension and improved mechanical environment in the microfluidic device could therefore lead to fewer spindle abnormalities and better chromosomal alignment, ultimately supporting healthier cell division outcomes.

Heated OoTrap also promotes increased rates of oocyte maturation and normal spindle

To enhance the portability and usability of the OoTrap device, especially for field-based applications, we designed a smaller version that incorporated a nichrome wire for heating, the heated OoTrap. The fabrication process was similar to that of the first OoTrap where a design (Fig. 4a) was made, and two moulds were 3D printed for subsequent PDMS casting (Fig. 4b). This modification allowed the OoTrap to maintain the necessary temperature for oocyte maturation without requiring an incubator. In microfluidic devices, various methods have been used for heating PDMS structures, such as external heaters, Peltier devices, exothermic chemical reactions and integrated resistive heaters (reviewed by ref. 46 and 47). It is important to note that PDMS has a thermal conductivity of approximately 0.15 W $(m\ K)^{-1}$ and a specific heat capacity of about 1.46 J $(g\ K)^{-1}$. These properties mean that while PDMS can maintain a stable temperature once heated, its low thermal conductivity makes it a poor conductor of heat. This low thermal conductivity can lead to slow and uneven heating, which is a drawback for applications requiring rapid and uniform temperature control.[48] The overall design of the heated OoTrap, incorporating nichrome wire in a flower-shaped pattern that covers most of the device's surface, both on the top and bottom, mitigated these limitations by providing localised and efficient heating as shown in Fig. 4c.

We chose to use joule heating using a nichrome wire due to its simplicity in fabrication and ability to provide localised and efficient heating. Joule heating works by passing an electric current through the nichrome wire, generating heat due to the wire's resistance.[49] This method is easy to implement and cost-effective, making it suitable for portable applications. To ensure stable temperature maintenance, we adapted the voltage supplied to each individual device. As shown in Fig. 4d, using the nichrome wire, the OoTrap's temperature was consistently kept within the range of 38.1–38.5 °C, achieving this desired temperature stability in approximately 35 minutes.

To further enhance the device's portability and affordability, a 3D-printed pump was integrated into the system (Fig. S1†). This modification reduced costs and made the OoTrap fully operational in field settings without needing additional laboratory equipment (Table S5†). Differently from what we initially calculated, the delay between steps had to be reduced from 29 696 ms to 20 500 ms to achieve a flow rate of 20 μL h^{-1} (0.001 mm s^{-1}). This is likely due to the precision of our 3D-printer that has changed the original dimensions of the pump gears, which can, in turn, affect the calculations. Therefore, care should be taken when using such devices, and flow rates should always be checked before using a new 3D-printed pump.

Due to the smaller dimensions of the heated OoTrap, we re-calculated the shear stress, which had an average of 0.7827 dyne cm^{-2}, with a maximum of 2.878 and a minimum of 0.000439 dyne cm^{-2}. It is important to note that the max shear stress values were only observed in the top of the microwell, in the surface of the channel (Fig. S2†), therefore, the oocyte would only encounter this possible detrimental shear stress if it was in the main channel or on the surface of the microwell.

We then tested this independent device by *in vitro* maturing non-selected COCs without using an incubator or any other lab equipment. Remarkably, we achieved higher maturation rates than the control group: 63.57 ± 9.87 *vs.* 41.67 ± 3.05 ($p < 0.0001$; n = 171 and 169, respectively, analysis performed in 3 replicates) demonstrating the effectiveness of the heated OoTrap (Fig. 4e). We also examined spindle morphology and chromosome alignment abnormalities in MII oocytes across the different treatment groups. Similarly to the bigger OoTrap, the heated OoTrap perfusion (n = 52) group also exhibited lower abnormalities at 7.00 ± 10.95% compared to the 2D (n = 88) at 25.09 ± 19.36 (Fig. 4f).

Studies focusing on performing IVM outside of an incubator do so by using portable incubators without CO_2 control (Table S6†) and were already described for ovine,[50] bovine,[51] porcine[52] and equine[51] IVM. Similarly to our heated OoTrap, these studies have shown no negative effects of the lack of CO_2 control on oocyte maturation rates. As detailed in Table S6,† culture media was supplemented or adjusted to ensure successful IVM despite the absence of CO_2 control. It is important to note that while these studies still required a portable incubator for temperature control, along with a stereomicroscope and trained personnel for oocyte handling, our heated OoTrap does not require such equipment. These enhancements make the heated OoTrap a practical and cost-effective solution for oocyte IVM, particularly in settings where traditional laboratory infrastructure is unavailable.

To enhance the portability of the heated OoTrap, we developed and 3D-printed a custom transportation box designed to securely house both the electrical and non-electrical components, making it well-suited for use in field or farm conditions (Fig. 4g and h; Video S1†). The box consists of two layers: the lower chamber holds the heated OoTrap, protecting it from light and creating a humidified environment essential for preventing media evaporation and bubble formation within the device. Additionally, the system is fully powered by a portable power bank, ensuring flexibility in remote settings. The PDMS device is easily detachable and re-connectable, and is reusable after proper cleaning with sterile water and detergents, followed by sterilization procedures. This design promotes efficient, field-ready use while maintaining sterility and functionality.

Conclusions

The development and use of OoTrap represent a significant contribution to ART. Using 3D printed moulds enabled rapid and cost-effective production of PDMS devices, addressing the traditional challenges of mould fabrication. Through optimised protocols, we ensured proper PDMS curing, producing high-quality devices suitable for biological applications, with the OoTrap demonstrating effective nutrient diffusion and waste removal, crucial for maintaining optimal culture conditions. OoTrap's perfusion setup can introduce important mechanical stimulation to the COCs, providing a more favourable environment for oocyte maturation. IVM experiments confirmed its superior performance, with significantly higher oocyte maturation rates and better spindle integrity compared to conventional 2D and static culture systems. By incorporating a nichrome wire heating system, the OoTrap maintained the necessary temperature for IVM without requiring an incubator, enhancing its portability and field usability. The use of a 3D-printed pump and a custom transport box, further supported its use in resource-limited and field-based settings, making it a practical and versatile tool for ART, offering a robust, cost-effective, and efficient solution for IVM, particularly in settings lacking traditional lab infrastructure.

Data availability

All data produced and analysed in this project are available within the main manuscript and as ESI.†

Author contributions

Conceptualization: all; methodology: all; investigation: all; supervision: MAMMF; writing – original draft: all; writing – review & editing: all authors.

Conflicts of interest

There are no conflicts to declare.

Acknowledgements

This work was supported by the Alexander von Humboldt Foundation in the framework of the Sofja Kovalevskaja Award (SKP 2020) endowed by the German Federal Ministry of Education and Research. We would like to thank G. A. F., P. K. F., M. C. and A. E. S. V. for helping with oocyte aspiration during experiments.

References

1 C. De Geyter, C. Calhaz-Jorge, M. S. Kupka, C. Wyns, E. Mocanu, T. Motrenko, G. Scaravelli, J. Smeenk, S. Vidakovic, V. Goossens and The European IVF-monitoring Consortium (EIM) for the European Society of Human Reproduction and Embryology (ESHRE), *Hum. Reprod. Open*, 2020, **2020**, hoz038.

2 G. M. Chambers, S. Dyer, F. Zegers-Hochschild, J. de Mouzon, O. Ishihara, M. Banker, R. Mansour, M. S. Kupka and G. D. Adamson, *Hum. Reprod.*, 2021, **36**, 2921–2934.

3 J. R. Herrick, *Biol. Reprod.*, 2019, **100**, 1158–1170.

4 T. B. Hildebrandt, S. Holtze, S. Colleoni, R. Hermes, J. Stejskal, I. Lekolool, D. Ndeereh, P. Omondi, L. Kariuki, D. Mijele, S. Mutisya, S. Ngulu, S. Diecke, K. Hayashi, G. Lazzari, B. De Mori, P. Biasetti, A. Quaggio, C. Galli and F. Goeritz, *Reproduction*, 2023, **166**, 383–399.

5 F. Goeritz, J. Painer, K. Jewgenow, R. Hermes, K. Rasmussen, M. Dehnhard and T. Hildebrandt, *Reprod., Fertil. Dev.*, 2012, **47**, 156–160.

6 R. Nosrati, *Lab Chip*, 2022, **22**, 1680–1689.

7 S. Le Gac, M. Ferraz, B. Venzac and P. Comizzoli, *Trends Biotechnol.*, 2021, **39**, 584–597.

8 R. C. Sequeira, T. Criswell, A. Atala and J. J. Yoo, *Tissue Eng. Regener. Med.*, 2020, **17**, 787–800.

9 G. A. Ferronato and M. A. M. M. Ferraz, *Anim. Reprod.*, 2023, **20**(2), e20230058.

10 C. Han, Q. Zhang, R. Ma, L. Xie, T. Qiu, L. Wang, K. Mitchelson, J. Wang, G. Huang, J. Qiao and J. Cheng, *Lab Chip*, 2010, **10**, 2848–2854.

11 A. Mastrorocco, L. Cacopardo, L. Temerario, N. A. Martino, F. Tridente, A. Rizzo, G. M. Lacalandra, D. Robbe, A. Carluccio and M. E. Dell'Aquila, *Cell*, 2022, **11**, 3611.

12 A. Mastrorocco, L. Cacopardo, D. Lamanna, L. Temerario, G. Brunetti, A. Carluccio, D. Robbe and M. E. Dell'Aquila, *Cell*, 2021, **10**, 1458.

13 Y. Yuan, M. Paczkowski, M. B. Wheeler and R. L. Krisher, *Reprod. Domest. Anim.*, 2014, **26**, 375.

14 M. Berenguel-Alonso, M. Sabés-Alsina, R. Morató, O. Ymbern, L. Rodríguez-Vázquez, O. Talló-Parra, J. Alonso-Chamarro, M. Puyol and M. López-Béjar, *SLAS Technol.*, 2017, **22**, 507–517.

15 M. Wang, T. Zhu, C. Liu, L. Jin, P. Fei and B. Zhang, *Biomed. Pharmacother.*, 2022, **154**, 113567.

16 S. Yadav, S. J. Shire and D. S. Kalonia, *Pharm. Res.*, 2011, **28**, 1973–1983.

17 S. A. M. van Stroe-Biezen, F. M. Everaerts, L. J. J. Janssen and R. A. Tacken, *Anal. Chim. Acta*, 1993, **273**, 553–560.

18 C. Culbertson, *Talanta*, 2002, **56**, 365–373.

19 F. Hartig, DHARMa: Residual Diagnostics for Hierarchical ## (Multi-Level/Mixed) Regression Models, *R package version 0.4.6. ## (version 0.4.6)*, **http://florianhartig.github.io/DHARMa/**, 2022.

20 B. Venzac, S. Deng, Z. Mahmoud, A. Lenferink, A. Costa, F. Bray, C. Otto, C. Rolando and S. Le Gac, *Anal. Chem.*, 2021, **93**, 7180–7187.

21 M. de Almeida Monteiro Melo Ferraz, H. H. W. Henning, P. F. da Costa, J. Malda, S. Le Gac, F. Bray, M. B. M. van Duursen, J. F. Brouwers, C. H. A. van de Lest, I. Bertijn, L. Kraneburg, P. L. A. M. Vos, T. A. E. Stout and B. M. Gadella, *Environ. Sci. Technol. Lett.*, 2018, **5**, 80–85.

22 M. de A. M. M. Ferraz, J. Beth, V. Bastien, M. de Almeida Monteiro Melo Ferraz, J. B. Nagashima, B. Venzac, S. Le Gac and N. Songsasen, *Sci. Rep.*, 2020, **10**, 1–9.
23 Y. Xie, F. Wang, W. Zhong, E. Puscheck, H. Shen and D. A. Rappolee, *Biol. Reprod.*, 2006, **75**(1), 45–55.
24 M. A. M. M. Ferraz, H. S. Rho, D. Hemerich, H. H. W. W. Henning, H. T. A. van Tol, M. Hölker, U. Besenfelder, M. Mokry, P. L. A. M. Vos, T. A. E. Stout, S. Le Gac and B. M. Gadella, *Nat. Commun.*, 2018, **9**, 4934.
25 S. C. Goh, Y. Luan, X. Wang, H. Du, C. Chau, H. E. Schellhorn, J. L. Brash, H. Chen and Q. Fang, *J. Mater. Chem. B*, 2018, **6**, 940–949.
26 J. Hawkins, X. Miao, W. Cui and Y. Sun, *J. R. Soc. Interface*, 2022, **19**, 20210929.
27 M. Gonçalves, I. M. Gonçalves, J. Borges, V. Faustino, D. Soares, F. Vaz, G. Minas, R. Lima and D. Pinho, *Polymer*, 2024, **16**, 1416.
28 A. Biswas, B. H. Ng, V. S. Prabhakaran and C. J. Chan, *Front. Cell Dev. Biol.*, 2022, **10**, 1038107.
29 Z. Rashidi, M. Azadbakht, A. Amini and I. Karimi, *Cell J.*, 2014, **15**, 282–293.
30 E. Farge, in *Current Topics in Developmental Biology*, Elsevier, 2011, vol. 95, pp. 243–265.
31 Z. Rashidi, M. Azadbakht and M. Khazaei, *Iran. J. Reprod. Med.*, 2012, **10**, 257–264.
32 S. L. Angione, N. Oulhen, L. M. Brayboy, A. Tripathi and G. M. Wessel, *Fertil. Steril.*, 2015, **103**, 281–290.e5.
33 C. Fang, F. Ji, Z. Shu and D. Gao, *Lab Chip*, 2017, **17**, 951–960.
34 X. Guo, Z. Chen, K. Memon, X. Chen and G. Zhao, *Cryobiology*, 2019, **92**, 267–271.
35 Y. Guo, Y. Yang, X. Yi and X. Zhou, *Cryobiology*, 2019, **90**, 63–70.
36 Y. S. Heo, H. J. Lee, B. A. Hassell, D. Irimia, T. L. Toth, H. Elmoazzen and M. Toner, *Lab Chip*, 2011, **11**, 3530–3537.
37 D. Lai, J. Ding, G. W. Smith, G. D. Smith and S. Takayama, *Hum. Reprod.*, 2015, **30**(1), 37–45.
38 B. Sadeghzadeh Oskouei, M. Pashaiasl, M. H. Heidari, M. Salehi, H. Veladi, F. Ghaderi Pakdel, P. Shahabi and M. G. Novin, *Cell J.*, 2016, **18**, 205–213.
39 B. Sadeghzadeh Oskouei, S. Zargari, P. Shahabi, M. Ghaffari Novin and M. Pashaiasl, *Cell J.*, 2021, **23**, 32–39.
40 E. M. Walters, D. J. Beebe and M. B. Wheeler, *Theriogenology*, 2001, **54**, 497.
41 W.-H. Wang, L. Meng, R. J. Hackett, R. Odenbourg and D. L. Keefe, *Fertil. Steril.*, 2001, **75**, 348–353.
42 L. Tilia, M. Chapman, S. Kilani, S. Cooke and C. Venetis, *Fertil. Steril.*, 2020, **113**, 105–113.e1.
43 S. M. Larson, H. J. Lee, P. Hung, L. M. Matthews, D. N. Robinson and J. P. Evans, *Mol. Biol. Cell*, 2010, **21**, 3182–3192.
44 J. P. Evans and D. N. Robinson, *Mol. Reprod. Dev.*, 2011, **78**, 769–777.
45 A. J. Maniotis, C. S. Chen and D. E. Ingber, *Proc. Natl. Acad. Sci. U. S. A.*, 1997, **94**, 849–854.
46 A. A. Dos-Reis-Delgado, A. Carmona-Dominguez, G. Sosa-Avalos, I. H. Jimenez-Saaib, K. E. Villegas-Cantu, R. C. Gallo-Villanueva and V. H. Perez-Gonzalez, *Electrophoresis*, 2023, **44**, 268–297.
47 V. Miralles, A. Huerre, F. Malloggi and M.-C. Jullien, *Diagnostics*, 2013, **3**, 33–67.
48 I. Maia, C. Rocha, P. Pontes, V. Cardoso, J. M. Miranda, A. S. Moita, G. Minas, A. L. N. Moreira, R. Lima, I. Maia, C. Rocha, P. Pontes, V. Cardoso, J. M. Miranda, A. S. Moita, G. Minas, A. L. N. Moreira and R. Lima, in *Advances in Microfluidic Technologies for Energy and Environmental Applications*, IntechOpen, 2020.
49 D. Erickson, D. Sinton and D. Li, *Lab Chip*, 2003, **3**, 141–149.
50 S. R. Byrd, G. Flores-Foxworth, A. A. Applewhite and M. E. Westhusin, *Theriogenology*, 1997, **47**, 857–864.
51 L. F. Campos-Chillon, C. M. Owen and J. L. Altermatt, *J. Equine Vet. Sci.*, 2019, **73**, 51–55.
52 K. W. Park, *Reproductive and Developmental Biology*, 2012, **36**(3), 141–145.

